STUDY OF ATMOSPHERIC FRONTS USING RISAT-1 SAR DATA OVER INDIAN OCEAN

Jagdish Prajapati[1, 2,*], Bipasha Paul Shukla[1, 2], Abhisek Chakraborty[1] and Raj Kumar[1]

[1]Earth, Ocean, Atmosphere, Planetary Sciences and Applications Area (EPSA),
Space Applications Centre (SAC),
Indian Space Research Organisation (ISRO),
Ahmedabad (Gujarat), India, Ph. +91-79-26914012
e-mail: jagdish.aug1991@gmail.com, bipasha@sac.isro.gov.in, abhisek1984@sac.isro.gov.in, rksharma@sac.isro.gov.in

[2]Department of Mathematics, Gujarat University, Ahmedabad, Gujarat, Ph. +91-79-26301154

Corresponding author e-mail: jagdish.aug1991@gmail.com

KEY WORDS: Normalized Radar Cross Section, Synthetic aperture radar, Wind Speed

ABSTRACT: Marine Atmospheric Boundary Layer (MABL) is the region where the ocean and the atmosphere exchange large amount of heat, moisture, and momentum, primarily via turbulent transport. There are several interesting atmospheric features like atmospheric gravity waves, convective cells, atmospheric fronts, rolls etc. which define and explain multi-scalar phenomena occurring in this layer. An important MABL feature, which we have considered here is the atmospheric front. Atmospheric fronts in the lower troposphere often mark regions of significant weather and those associated with extra-tropical cyclones are related to heavy precipitation events. The fronts producing extreme precipitation events are found to have stronger frontal gradients than other fronts, potentially providing some improved forecasting capabilities for extreme precipitation. The detection of atmospheric fronts is thus very important and is made possible by studying their imprints on the sea surface using backscatter radar echo. In the present study, we aim to detect atmospheric fronts over Indian Ocean using Radar Imaging Satellite-1 (RISAT-1) Synthetic Aperture Radar (SAR) data.

Atmospheric fronts are air mass boundaries that have collapsed down to near-zero order discontinuities in wind speed. They are often accompanied by a surface wind maximum along and just ahead of the front. The SAR signature of a front most often appears as a sharp gradient in SAR intensity. The typical frontal features were captured SAR images acquired by the RISAT-1 satellite over the Arabian sea and Bay of Bengal. In the present study ERA (ECMWF Regular Analysis)-Interim reanalysis data are used to compute thermal front parameter, and front points derived from them are overlaid on the SAR images depicting as the atmospheric fronts. The associated wind speed exhibits a sharp demarcation between the two regions, with the wind speed difference in the range of 2-4 m/s.

1.0 INTRODUCTION

Atmospheric fronts are boundaries between air masses. These air masses have different physical properties and are usually associated with different wind speeds on both sides of the front. Atmospheric fronts are important for the day-to-day variability of weather in the mid latitudes. It is therefore vital to know how their distribution and frequency will change in a projected warmer climate. They are associated with a large proportion of global rainfall [Catto et al., 2012], are often associated with extreme rain events [Catto and Pfahl, 2013], and can cause damaging flood events [Pitt, 2008]. These features are visible on SAR imagery because they leave a fingerprint on the sea surface by modifying the small-scale sea surface roughness generated by small wavelength capillary waves. Generally, as the sea roughness increases the backscattered radar power or the Normalized Radar Cross Section (NRCS) increases and thus lighter the gray tone in the SAR imagery [Valenzuela, 1978]. In general, the wind stress and thus the small-scale sea surface roughness change, across atmospheric fronts, become visible on SAR images as structured lines separating areas of differing NRCS values (or gray tones) in the SAR image. However, variations of the small-scale sea-surface roughness may also have other origins other than the variation of the wind stress [Alpers, 1995]. For example, variations of the surface current associated with oceanic fronts give rise to variations of the small-scale sea surface roughness due to wave-current interaction and thus to variations of the NRCS [Vesecky and Stewart, 1982; Lyzenga, 1991; Johannessen et al., 1996].

In the present study, an attempt has been made to identify the atmospheric fronts from RISAT-1 SAR data. This is done by utilizing ERA-Interim reanalysis data to compute thermal front parameter and other stability indices. The data used in the study is summarized in Section-II and the methodology is described in the Section-III. Finally, the result is discussed in Section-IV and the conclusion in Section-V.

2.0 DATA USED

Radar Imaging Satellite-1 (RISAT-1) is the India's first SAR mission, was launched on April 26, 2012 on-board PSLV-XL C19, carrying a C –band (5.35 GHz) synthetic aperture radar in a Sun-synchronous dawn–dusk orbit of altitude 536 km with inclination of 97.55° and orbital period of 95.5 min. This mission stands among other SAR missions to fill the data-gap in the coastal regions. RISAT-1 has come up with huge potential to monitor vegetation, atmospheric studies, coastal and cryosphere studies. It is designed to image the Earth's surface in different modes; HRS (High Resolution SPOTLIGHT mode), FRS-1 (Fine Resolution STRIPMAP mode), FRS-2 (Fine Resolution Alternate Polarization STRIPMAP mode), MRS (Medium Resolution SCANSAR mode) and CRS (Coarse Resolution SCANSAR mode) with variable swath widths ranging from 30 to 240 km. The payload system is configured to perform self-calibration of transmit and receive paths before and after imaging sessions through a special instrument calibration technique [Misra et al, 2016]. In the present study, RISAT-1 MRS images acquired at HH polarization on Jul 19, 2013 at 2351 UTC; Aug 13, 2015 at 0058 UTC and Jan 24, 2016 at 0048 UTC are used. Further corresponding ERA-Interim reanalysis data from the atmospheric model ECMWF (European Centre for Medium-Range Weather Forecasts) are used. In the frontal features extraction, temperature data at the pressure levels 700 hPa, 850 hPa and 1000 hPa are used to compute potential temperature and Lower Tropospheric Stability (LTS). LTS are generally related to low cloud region. The time lag between RISAT-1 and ERA data are 58 min, 09 min and 48 min for Aug 13, 2015; July 19, 2013 and Jan 24, 2016 respectively.

3.0 METHODOLOGY

Atmospheric features are identified in reflectivity with their impinging signature on sea surface. The detection of atmospheric fronts is based on the thermal front parameter analysis [Renard et. al, 1965] and Wind changes [Simmonds et al. 2012]. In the present study, we have analysed 2000 RISAT-1 SAR images over a period of (2012 – 2016) to locate potential candidates for atmospheric fronts. Further the images are then pre-processed and downscaled to 1 km to reduce noises and artefacts in the SAR imagery. As we know, radar reflectivity and speckle noises follow Gamma Function. Thus, the speckle noise in the SAR imagery were minimized using 7×7 Gamma Map filter [Gagnon et. al., 1997] and DN (Digital Number) values are then converted to NRCS(σ^0) using the relation

$$\sigma^0(dB) = 20\log_{10} DN - e + 10\log_{10}(\sin\theta\,/sin\beta) \tag{1}$$

where e is the product calibration constant, θ is the local incidence angle and β is the incidence angle of central pixel [RISAT-1 Data Product Format, 2015]. To understand the characteristics of MABL phenomena, we have converted the NRCS measurements to the sea surface wind field using the existing geophysical model functions (GMFs)—that is, the C-band Model Function, version 5 (CMOD5.N) [Hersbach, 2008 and Chakraborty et. al., 2013]. The signature of a front, most often appears as a sharp gradient in a SAR imagery. Typical frontal features were captured SAR images acquired by the RISAT-1 satellite over the Arabian Sea and Bay of Bengal on July 19, 2013; August 13, 2015 and January 24, 2016. Here, ERA-Interim reanalysis data is used to compute Thermal front parameter(TFP), and front points derived from them are overlaid on the SAR imagery depicting an atmospheric front. First, the thermal front parameter is calculated, defined by [Renard et. al.,1965] as

$$TFP(\zeta) = -\nabla|\nabla\zeta|.\left(\frac{\nabla\zeta}{|\nabla\zeta|}\right) \tag{2}$$

where ζ is a scalar thermodynamic variable (here the potential temperature). Further, we have also computed LTS (the difference between potential temperature at 700 hPa and 1000 hPa) and examined the sea surface temperature gradients using ECMWF ERA-Interim 12.5 km SST data. Frontal points are identified where the gradient of the thermal front parameter is zero.

4.0 RESULTS AND DISCUSSION

The key datum for this study is the RISAT-1 SAR images acquired on July 19, 2013 at 2351 UTC; August 13, 2015 at 0058 UTC and January 24, 2016 at 0048 UTC over the Arabian Sea and Bay of Bengal. These images are acquired in the

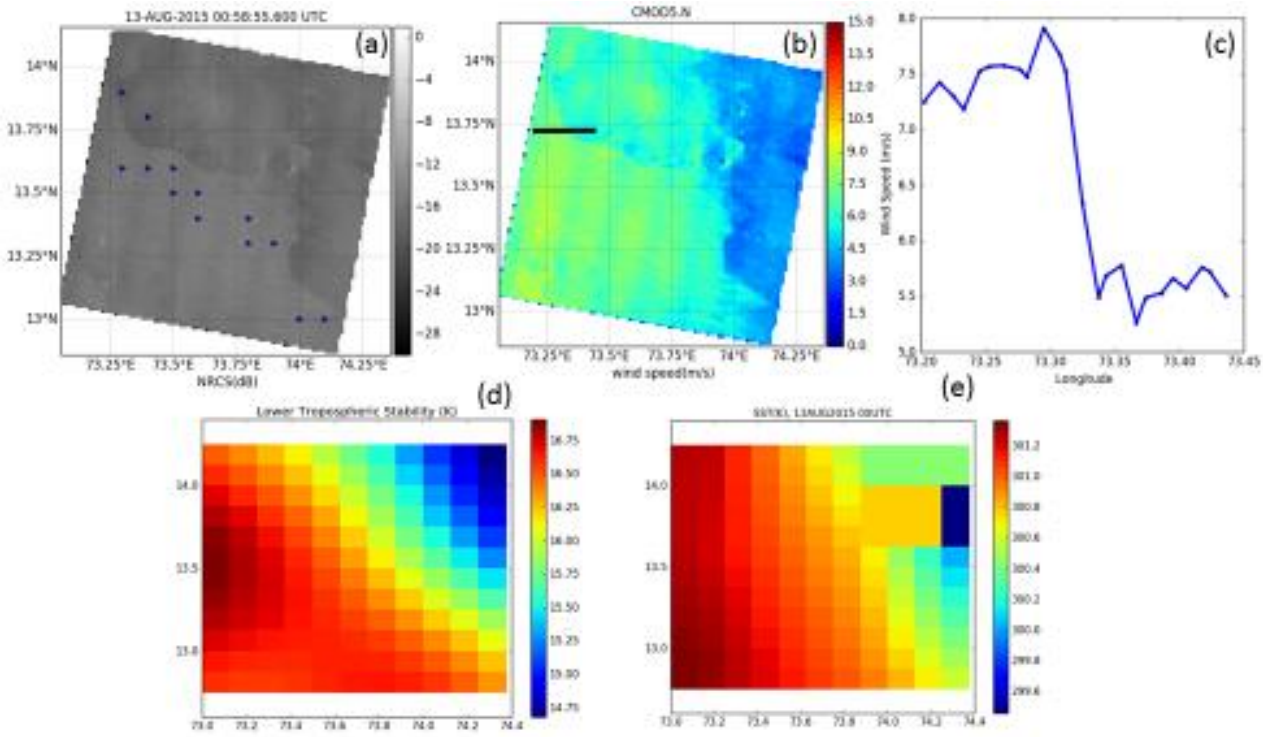

Figure 1: (a) Enhanced NRCS image acquired on Aug 13, 2015 at 0058 UTC (b) High resolution (1 km x 1 km) wind speed retrieved from RISAT-1 with Transect (Black Line), (c) Variation of wind speed along the transect, (d) Lower tropospheric stability on Aug 13, 2015 at 0000 UTC, (e) Sea Surface Temperature(SST).

Medium Resolution ScanSAR (MRS) imaging mode. The polarization of the RISAT-1 SAR is horizontal (HH) for transmission and for reception in the incidence angle range between 30 to 45 degree, each having a width of about 115 km and the spatial resolution of 18 m. Though the reanalysis used is relatively coarse, it can be observed that the derived fronts points are closely matching and aligned with the frontal features identified by visual inspection. The wind speed associated with the NRCS is also plotted Fig 1b, 2b and 3b. As expected, there is a sharp demarcation between the two regions, with the wind speed difference in the range of 2-4 m/s. Boundary layer stability is characterized using the measure proposed by [Klein et. al, 1993], called lower tropospheric stability (LTS). Boundary layer stability measures LTS of temperature. Results and Discussion are summarized in three different cases based on the data availability in the Indian Ocean.

4.1 Case 1: Arabian Sea

Figure 1a shows the enhanced NRCS image of RISAT-1 MRS mode acquired on August 13,2015. Blue arrows are the front points derived from the ERA-Interim potential temperature data, depicting as an atmospheric front. Fig 1c describes the variations of wind speed along the transect. The average maximum wind speed values across the transect shows the mean and standard deviation of 9.14 m/s and 0.62 m/s and the minimum wind speed shows the mean and standard deviation of 6.33 m/s and 0.30 m/s i.e. there is around 3 m/s difference in wind speed in the two region separated by the frontal boundary. In order to investigate, further we have analysed the LTS (Fig 1d), where two demarcated zones are observed. However, the SST (Fig 1e) gradients exhibit similar pattern, suggests ocean induced boundary layer front.

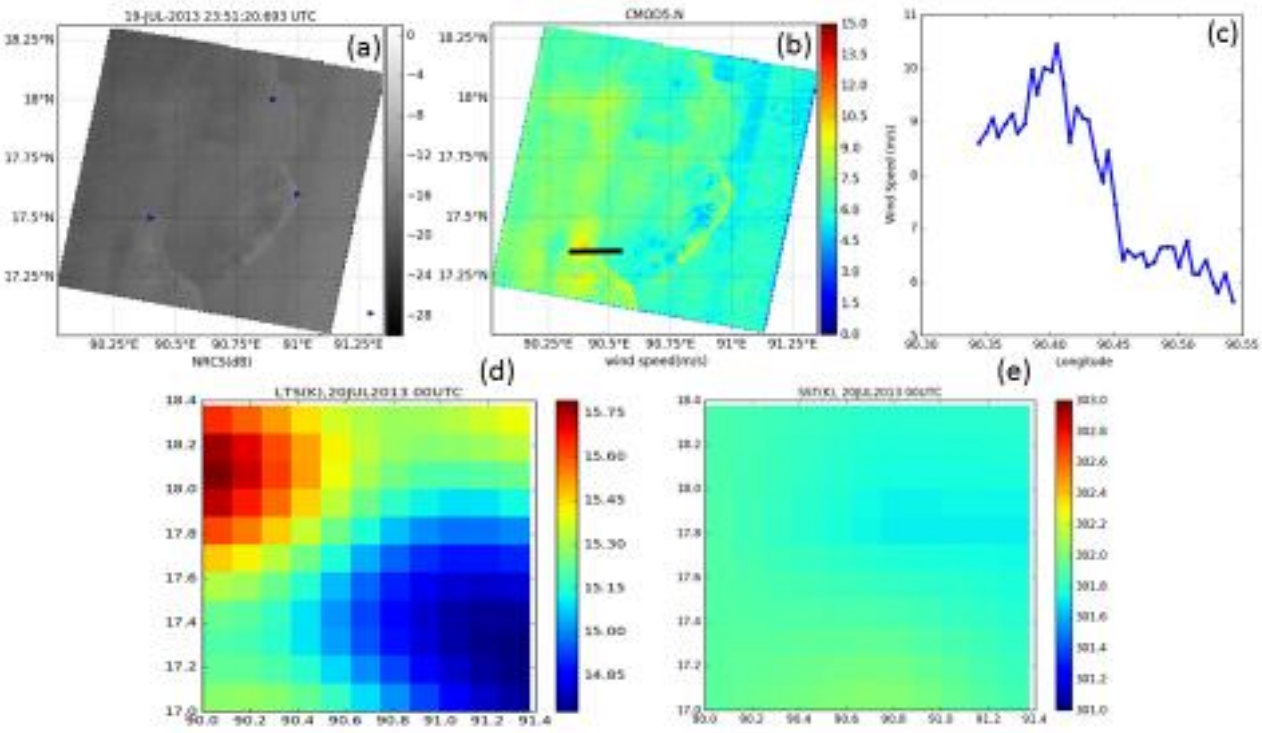

Figure 2: (a) Enhanced NRCS image acquired on July 19, 2013 at 2351 UTC (b) High resolution (1 km x 1 km) wind speed retrieved from RISAT-1 with Transect (Black Line), (c) Variation of wind speed along the transect, (d) Lower tropospheric stability on July 20, 2013 at 0000 UTC, (e) Sea Surface Temperature(SST).

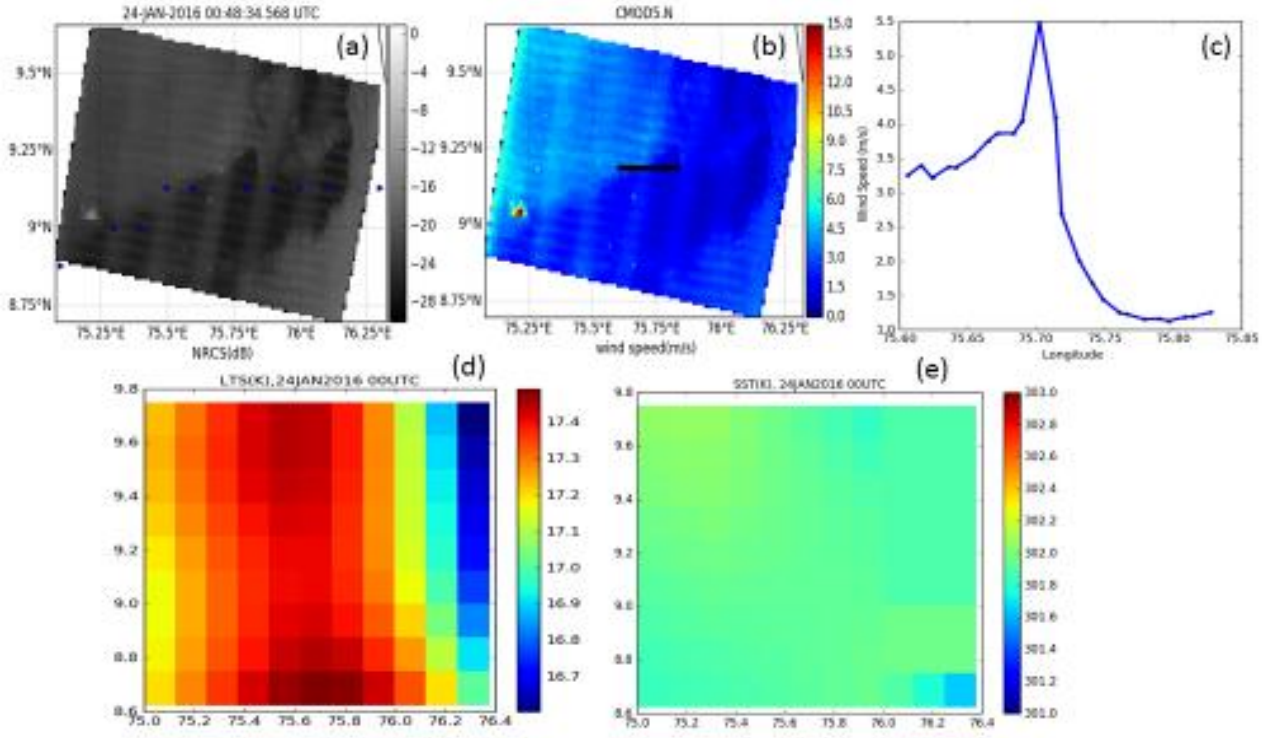

Figure 3: (a) Enhanced NRCS image acquired on Jan 24, 2016 at 0048 UTC (b) High resolution (1 km x 1 km) wind speed retrieved from RISAT-1 with Transect (Black Line), (c) Variation of wind speed along the transect, (d) Lower tropospheric stability on Jan 24, 2016 at 0000 UTC, (e) Sea Surface Temperature (SST).

4.2 Case 2: Bay of Bengal

The black line in Fig. 2b shows the transect, Fig 2c shows the variations of wind speed along the transect. Maximum wind speed along the transect shows the mean and the standard deviation of 7.49 m/s and 0.19 m/s and the minimum wind speed shows 5.59 m/s and 0.15 m/s respectively. Across the Fig 2d, shows the area with the lowest LTS values moves with respect to the cold front. The homogeneity of SST is showing a contrast behaviour as compared to case-1, which emphasises on atmospheric circulation induced frontogenesis.

4.3 Case 3: South Indian Ocean

Figure 3a and 3c shows the enhanced NRCS, wind speed and variation of wind speed in m/s along the transect, respectively. The maximum wind speed along the transect shows the mean and standard deviation of 3.5 m/s and 0.23 m/s and minimum wind speed along the transect shows the mean and standard deviation of 1.26 m/s and 0.16 m/s. The very less temperature difference and the LST difference less than 20K is an evidence of cold front.

5.0 CONCLUSION

The paper studies the atmospheric frontal signature using RISAT-1 SAR data. For this study a multitude of SAR images were analysed for detecting potential front structure. Apart from the wind speed and NRCS gradients we have also computed the thermal front parameter for pointing at front locations. Further in order to investigate the frontogenesis, an investigation on the spatial variation of SST and LTS was also carried out for the study region. Thus, in this paper we describe the cases of three different kinds of frontal signature. In all the three cases demarcated zones in SAR observed NRCS and Wind magnitude are observed. This is also validated with the presence of TFP in the region. However, it is seen that there are significant differences in the SST and LTS maps. For the case where air-sea interaction is anticipated the demarcated zones are presence in both LTS and SST maps, while for homogeneous SST and stratified LTS atmospheric circulation induced frontogenesis is hypothesized.

ACKNOWLEDGEMENTS

We would like to thank Shri Tapan Misra, Director, Space Applications Centre, Ahmedabad for their kind support. The authors are very thankful to National Remote Sensing Centre for providing RISAT-1 SAR data. Thanks are also extended to European Centre for Medium Range Weather Forecasts for their data support.

REFERENCES:

Alpers, W., 1995. Measurement of mesoscale oceanic and atmospheric phenomena by ERS-1 SAR. URSI Radio Sci. Bull., 275, pp. 14–22.

Catto, J. L., Jakob, C., Berry, G., and Nicholls, N., 2012. Relating global precipitation to atmospheric fronts. Geophys. Res. Lett., 39, L10805, doi:10.1029/2012GL051736.

Catto, J. L., and Pfahl, S., 2013. The importance of fronts for extreme precipitation. J. Geophys. Res. Atmos., 118, pp. 10,791–10,801. doi:10.1002/jgrd.50852.

Chakraborty M., S. Panigrahy S., Rajawat A. S., Kumar R., Murthy T.V.R., Haldar D., Chakraborty A., Kumar T., Rode S., Kumar H., and Mahapatra M., 2013. Initial results using RISAT-1 C-band SAR data. Current Science(Bangalore), 104(4), pp.490-501.

Gagnon, Langis, and Jouan A., 1997. Speckle filtering of SAR images: a comparative study between complex-wavelet-based and standard filters. In Optical Science, Engineering and Instrumentation'97, International Society for Optics and Photonics, pp. 80-91.

Hersbach, H., April 2008. CMOD5.N “A C-band geophysical model function for equivalent neutral wind. Tech. Rep. TR, ECMWF, ECMWF technical Memorandum 554.

Johannessen, J. A., Shuchman, R., Digranes, A. G., Lyzenga, D. R., Wackerman, C., Johannessen, O. M., and Vachon, P. W., 1996. Coastal ocean fronts and eddies imaged with ERS-1 synthetic aperture radar. J. Geophys. Res., 101(C3), pp. 6651–6667.

Klein, S. A., and D. L. Hartmann, 1993. The seasonal cycle of low stratiform clouds. J. Climate, 6, pp. 1587–1606, doi:10.1175/1520-0442(1993)006,1587:TSCOLS.2.0.CO;2.

Lyzenga, D. R., 1991. Interaction of short surface and electromagnetic waves with ocean fronts. J. Geophys. Res., 96(C6), pp. 10,765–10,772.

Misra T., Bhan, R., Putrevu, D., Mehrotra, P., Nandy, P. S., Shukla, S. D., Rao, C. V. N., Dave, D. B., and Desai, N. M., 2016. Instrument calibration architecture of Radar Imaging Satellite (RISAT-1), In Proc.SPIE –In International Society for Optics and Photonics, 9876, pp. 98811A-98811A.

Pitt, M., 2008. The Pitt review—Lessons learned from the 2007 summer floods, Final Rep., Cabinet Office, London, U. K.

Renard, R. J., and Clarke L. C., 1965. Experiments in numerical objective frontal analysis, Mon. Wea. Rev., 93, pp. 547–556.

RISAT-1 Data Products Format, Version 1.4, September 2015, Space Applications Centre, (ISRO). Retrieved Aug, 29, 2017, from https://www.nrsc.gov.in/sites/all/pdf/format3.pdf .

Simmonds, I., K. Keay, and Bye, J. A. T., 2012. Identification and climatology of Southern Hemisphere mobile fronts in a modern reanalysis. J. Climate, 25, pp. 1945–1962, doi:10.1175/JCLI-D-11-00100.1.

Valenzuela, G. R., 1978. Theories for interaction of electromagnetic and oceanic waves—A review. Boundary Layer Meteorol., 13, pp. 61–85.

Vesecky, J. F., and Stewart, R. H. 1982. The observations of ocean surface phenomena using imagery from the SEASAT synthetic aperture radar: An assessment. J. Geophys. Res., 87(C5), pp. 3397–3430.